Infection, Genetics and Evolution 87 (2021) 104672

Contents lists available at ScienceDirect

Infection, Genetics and Evolution

journal homepage: www.elsevier.com/locate/meegid

Research paper

Deep sequencing of the transcriptome from murine lung infected with H5N8 subtype avian influenza virus with combined substitutions I283M and K526R in PB2 gene

Sujuan Chen [a,b,c,1], Xiao Wang [a,b,c,1], Xiang Su [a,b,c], Xinyu Miao [a,b,c], Tao Qin [a,b,c], Daxin Peng [a,b,c,*], Xiufan Liu [a,b,c]

[a] College of Veterinary Medicine, Yangzhou University, Jiangsu Co-Innovation Center for the Prevention and Control of Important Animal Infectious Disease and Zoonoses, Yangzhou, Jiangsu 225009, PR China
[b] Joint International Research Laboratory of Agriculture and Agri-Product Safety, The Ministry of Education of China, Yangzhou, Jiangsu 225009, PR China
[c] Jiangsu Research Centre of Engineering and Technology for Prevention and Control of Poultry Disease, Yangzhou, Jiangsu 225009, PR China

ARTICLE INFO

Keywords:
Avian influenza virus
H5N8
PB2
Pathogenic mechanism
RNA-seq

ABSTRACT

H5N8 subtype highly pathogenic avian influenza viruses (HPAIVs) pose a huge threat to poultry industry and general public health. Our previous study demonstrated that synergistic effect of 283M and 526R in PB2 gene was a critical factor for viral high pathogenicity in mammals. However, the potential pathogenic mechanism of the mutant virus is still unclear. Here, RNA-seq method was used to analyze the global host response of murine lungs after infecting with parental r-JY virus and JY-PB2-I283M-K526R mutant virus. We found that both amounts and the expression levels of host differentially expressed genes (DEGs) were higher in mutant virus-infected mice compared with the group of parental virus. Furthermore, the DEGs mainly related with innate immune response by GO and KEGG analysis. Especially, PB2-I283M-K526R mutation strongly induced a sharp expression of cytokine storm-related genes, including MX1, CXCL10, and IFN-γ, performed by qRT-PCR. We also found that PB2-I283M-K526R mutation accelerated the level of cell apoptosis by heat map analysis of apoptosis-related DEGs in lungs and apoptosis assay *in vitro*. Taken together, our data demonstrated that PB2-I283M-K526R of H5N8 subtype HPAIV exacerbated the innate immune response and the level of cell apoptosis, which might be a key pathogenic mechanism for the enhanced pathogenicity of mutants in mammals.

1. Introduction

Highly pathogenic avian influenza (HPAI) H5N1 viruses have spread across Asia, Europe, and Africa. From 2003 to March 2020, 861 human cases have been confirmed, with a mortality rate of almost 52.8% (WHO/GIP, 2020). Recently, the H5N1 viruses evolved into novel reassortant H5Nx viruses with different neuraminidase (NA) genes, including H5N2, H5N6, and H5N8 subtypes, in which the novel H5N8 viruses distribute globally (Global Consortium for and Related Influenza, 2016). Therefore, it is crucial to understand the viral pathogenesis of H5N8 viruses and identify their virulence markers. Our previous study revealed that two genetically similar HPAI H5N8 viruses displayed a completely different virulence in mice. The HPAI H5N8 virus A/goose/Eastern China/CZ/2013 (CZ) was highly virulent, whereas HPAI H5N8 virus A/duck/Eastern China/JY/2014 (JY) was low virulent (Wang et al., 2016). Further study demonstrated that synergistic effect of amino acid residues 283M and 526R in PB2 was responsible for high virulence of the HPAI H5N8 virus in mice (Wang et al., 2017) in an etiological perspective. However, the mammalian pathogenesis induced by HPAI H5N8 virus with PB2-I283M-K526R mutation is still unclear.

The host response post virus infection contributes to the pathogenicity of H5 subtype AIVs. Clinical data suggested that virus-induced cytokine dysregulation is considered as one of contributory factor to the pathogenesis of H5 subtype AIVs (Baskin et al., 2009; Cameron et al., 2008; Perrone et al., 2008; Szretter et al., 2007). In humans, the lungs of H5N1 virus-infected patients had an aberrant host response, which was

* Corresponding author at: College of Veterinary Medicine, Yangzhou University, Jiangsu Co-Innovation Center for the Prevention and Control of Important Animal Infectious Disease and Zoonoses, Yangzhou, Jiangsu 225009, PR China.
E-mail address: pengdx@yzu.edu.cn (D. Peng).
[1] Sujuan Chen and Xiao Wang contributed equally to this work.

https://doi.org/10.1016/j.meegid.2020.104672
Received 11 June 2020; Received in revised form 13 November 2020; Accepted 6 December 2020
Available online 9 December 2020

evidenced by high levels of pro-inflammatory cytokine and chemokine expressions in primary human macrophages (de Jong et al., 2006; Peiris et al., 2004; Zhang et al., 2018). A better understanding of the global gene changes during infection will help develop the potential therapeutic strategies for emerging infectious diseases. Therefore, it is necessary to determine the global gene levels of mice infected with parental virus (r-JY) or mutant virus (JY-PB2-I283M-K526R) to further reveal the pathogenic mechanism of H5N8 virus infection. RNA sequencing (RNA-seq) technology, which is a powerful tool to profile the transcriptome with high efficiency and accuracy, has revealed insights into molecular mechanisms of various viral infections and diseases (Juranic Lisnic et al., 2013; Mei et al., 2014; Park et al., 2015; Wang et al., 2014; Zhang et al., 2018). RNA-seq offers both single-base resolution for annotation and "digital" gene expression levels at the genome scale, often at a much lower cost than either microarray or large-scale Sanger EST sequencing (Cloonan et al., 2008; Mortazavi et al., 2008). For example, RNA-seq method was used to reveal the systemic transcriptome responses of the murine lungs infected by swine (Jia6/10) or human (LN/09) H1N1/2009 viruses (Zou et al., 2013). Therefore, the global host response changes post H5N8 virus infection are needed to overall understand by using RNA-seq technology.

Herein, we used the RNA-seq technology to comprehensively annotate the host transcriptomes following infection to mice with H5N8 parental virus and PB2-I283M-K526R mutant virus. Our work will provide a global host response changes for illustrating the mammalian pathogenesis during infection of H5N8 subtype AIV with novel mutations.

2. Materials and methods

2.1. Ethics statement

The Jiangsu Administrative Committee for Laboratory Animals (Permission number: SYXKSU-2007-0005) approved all of the animal studies according to the guidelines of Jiangsu Laboratory Animal Welfare and Ethical of Jiangsu Administrative Committee of Laboratory Animals. All experiments involving live viruses and animals were performed in the authorized animal biosafety level 3 (ABSL-3) facilities at Yangzhou University.

2.2. Virus

JY virus (A/duck/Eastern China/JY/2014) was isolated from a dead duck. As a previous report, this virus belongs to clade 2.3.4.4, which is a newly evolved clade (Wang et al., 2016). Reverse genetic-derived JY (r-JY) was successfully generated previously (Wang et al., 2017). Recombinant viruses harboring mutations I283M plus K526R in the PB2 gene that increase virulence in mice was also generated. PB2 derived plasmids were sequenced to verify the presence of the introduced mutations and the absence of additional mutations.

2.3. Samples

6-week-old BALB/c mice ($n = 3$/group) were intranasally inoculated with 50 μL $10^{6.0}$ 50% embryo infectious doses (EID_{50}) of r-JY or JY-PB2-I283M-K526R. The mice of control group were inoculated with the same dosage of PBS. Transcriptional profiles were determined by the high-throughput RNA-seq analysis of lung tissues at 3 days post-infection (d. p. i.).

2.4. RNA quality examination, library preparation, and sequencing

RNA quality was examined by analysis of RNA purity by NanoDrop® spectrophotometers (Thermo Fisher, MA, USA) and rRNA band integrity using the RNA Nano 6000 assay kit based on the Bioanalyzer 2100 system (Agilent Technologies, CA, USA). A total amount of 1 μg qualified RNA per sample was used as input material for the library preparation. The sequencing libraries were generated using the VAHTS mRNA-seq v2 Library Prep kit for Illumina® (Vazyme, NR601, China) following manufacturer's recommendations. Firstly, mRNA was purified from total RNA by using the poly-T oligo-attached magnetic beads. Fragmentation was performed using divalent cations under elevated temperature in Vazyme Frag/Prime Buffer. The cleaved RNA fragments were copied into first strand cDNA using reverse transcriptase and random primers. Second strand cDNA synthesis was subsequently performed by using buffer, dNTPs, DNA polymerase I, and RNase H. Then, the cDNA fragments were end repaired with the addition of a single 'A' base at the 3'-end of each strand, ligated with the special sequencing adapters (Vazyme, N803, China) subsequently. Next, in order to acquire an appropriate size for sequencing, the products were purified and their size was selected by VAHTSTM DNA Clean Beads (Vazyme, N411, China). PCR was performed and aimed products were purified finally. The clustering of the index-coded samples was performed on a cBot Cluster Generation System (Illumia, USA) according to the manufacturer's instructions. After cluster generation, the library preparations were sequenced on an Illumina HiSeq 2500 (Illumina, San Diego, CA, USA).

2.5. The processing and analysis of transcriptional data

The raw reads were filtered by removing reads containing adapter, ploy-N and low-quality reads for subsequent analysis. The steps of sequencing data filtering: 1) removing reads containing adapter; 2) removing reads containing ploy-N (i.e., unrecognized bases), reads with a ratio greater than 5%; 3) removing low-quality reads (the number of bases which is $Q \leq 10$ is more than 50% of the entire read); All the downstream analyses were based on clean data with high quality. The reference genome and gene model annotation files were downloaded directly from the genome website (GenBank accession number: GCA_000001635.8). The reference genome index was built by using Bowtie2 (v2.2.9), and paired-end clean reads were aligned to the reference genome by using TopHat (v2.1.1). Software for adaptor trimming is SOAPnuke1.3.0. The mapped reads of each sample were assembled by using Cufflinks (v2.2.1) (Trapnell et al., 2012) with a reference-based approach. This method employed spliced reads to determine exon connectivity. Cufflinks uses a probabilistic model to simultaneously assemble and quantify the expression levels of a minimal set of isoforms, which provides a maximum likelihood explanation of the expression data in a given locus. Cuffdiff (v2.2.1) (Li et al., 2017) was used to calculate the expected number of fragments per kilobase of transcript sequence per millions base pairs sequenced (FPKMs) for coding genes in each sample. Gene FPKMs were computed by summing the FPKMs of the transcripts in each gene group. Cuffdiff (v2.2.1) (Ma et al., 2018) also provides statistical routines for determining differential expression in digital transcript or gene expression datasets by using a model based on a negative binomial distribution. False discovery rates (FDR) ≤ 0.001 and the absolute value of the log2Ratio ≥ 1 were used as a threshold to judge the statistical significance of gene expression.

2.6. GO and KEGG enrichment analysis

GO (Gene Ontology) enrichment analysis of differentially expressed genes was implemented with per module (GO::TermFinder). GO terms with corrected p value less than 0.05 were considered to be significantly enriched among the differentially expressed genes. KEGG (Kyoto Encyclopedia of Genes and Genomes) pathways with corrected p value less than 0.05 were considered to be significantly enriched among the differentially expressed genes (DEGs). The analyses were performed with DAVID (Database for Annotation, Visualization and Integrated Discovery, http://david.abcc. ncifcrf.gov/).

Table 1
Primers for the representative gene amplification.

Gene	Accession number	Primer name	Primer sequence (5′-3′)
CXCL10	NM_021274.2	CXCL10-F	CCAAGTGCTGCCGTCATTTTC
		CXCL10-R	GGCTCGCAGGGATGATTTCAA
IL-6	NM_031168.2	IL-6-F	TGAGATCTACTCGGCAAACCTAGTG
		IL-6-R	CTTCGTAGAGAACAACATAAGTCAGATACC
MX1	NM_010846.1	MX1-F	GACCATAGGGGTCTTGACCAA
		MX1-R	AGACTTGCTCTTTCTGAAAAGCC
IL-1β	NM_008361.4	IL-1β-F	GAATCTATACCTGTCCTGTG
		IL-1β-R	TTATGTCCTGACCACTGTTG
DHX58	NM_030150.2	DHX58-F	CAGGCGCATGCTGGATAAAC
		DHX58-R	CTCAGAGCTGTTGAGTGCCA
IFN-β	NM_010510.1	IFN-β-F	GATCCCTATGGAGATGACGGAGA
		IFN-β-R	ATTCCACCCAGTGCTGGAGA
IFN-γ	NM_008337.4	IFN-γ-F	AACTCAAGTGGCATAGATGTGGAAG
		IFN-γ-R	TGTTGACCTCAAACTTGGCAATAC
TNF-α	NM_013693.3	TNF-α-F	CCCTCACACTCAGATCATCTTCT
		TNF-α-R	GCTACGACGTGGGCTACAG
CD209b	NM_026972.5	CD209b-F	TGATGGTCAGCGGCAGCAGGTAT
		CD209b-R	GGAGCCCAGCCAAGAACAGGAAG
GSTA2	NM_008182.3	GSTA2-F	ATTTGATGTTTGACCAAGTGCCC
		GSTA2-R	TATTTGGTGGCGATGTAGTTGAGAAT
SCGB3A2	NM_001289643.1	SCGB3A2-F	TTTGGACGACATTATTCCCTCAT
		SCGB3A2-R	AGGTTGTTCACGTAGCAAAGGCT
β-actin	NM_007393.5	β-actin-F	CATCCGTAAAGACCTCTATGCCAAC
		β-actin-R	ATGGAGCCACCGATCCACA

2.7. qRT-PCR of innate immune-related genes

According to the result of RNA-seq, the representative innate immune-related genes, including interleukin-6 (IL-6), MX-1, CXCL10, TNF-α, IFN-β, IFN-γ, DHX58, GSTA2, and SCGB3A2 were verified by qRT-PCR. For real-time PCR, ABI 7500 Real-Time PCR System (Applied biosystem, Carlsbad, California, USA) and SYBR Green Master (Takara, Otsu, Japan) were used. Each sample and negative controls were run in at least three technical replicates. Gene-specific primers were designed and listed in Table 1. β-actin was amplified under the same conditions as internal control to normalize reactions. The expression value of each gene, relative to that for β-actin, was calculated using the $2^{-\triangle\triangle CT}$ method (Schmittgen et al., 2000).

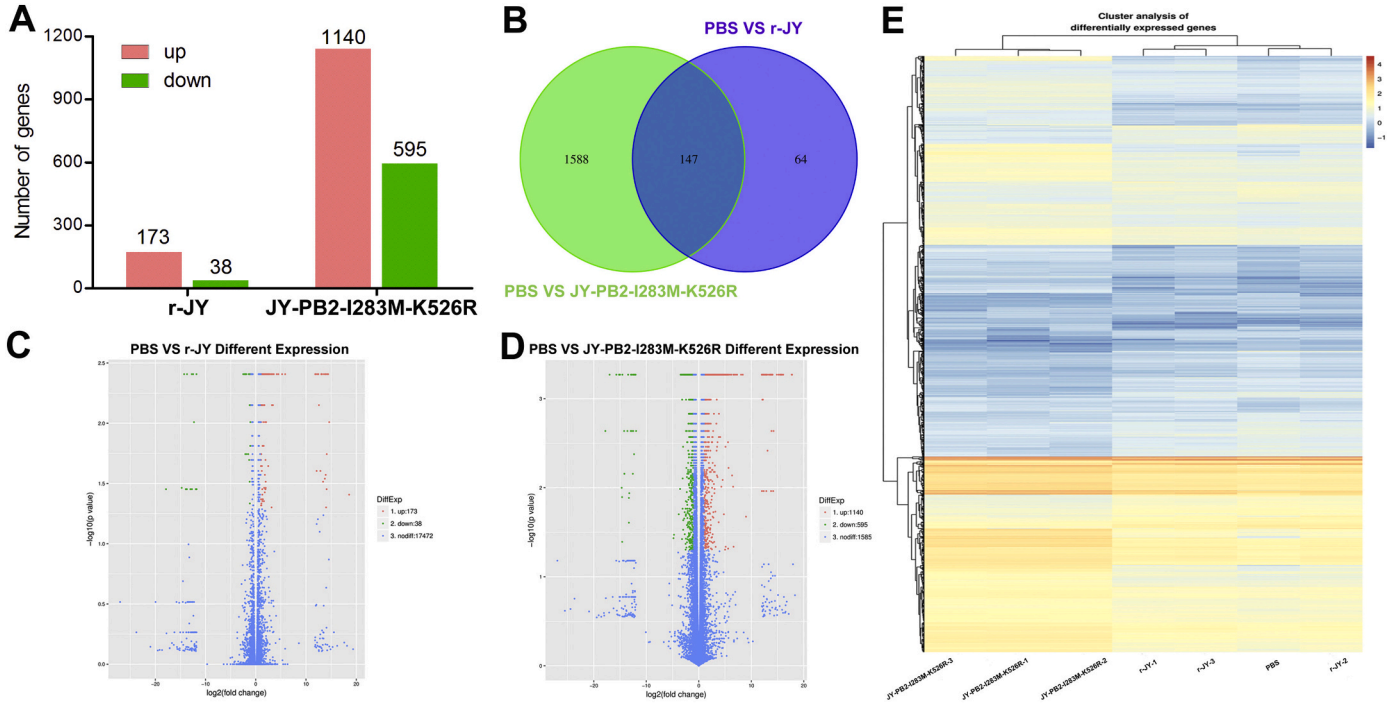

Fig. 1. Differences in gene expression between lungs from r-JY- and JY-PB2-I283M-K526R-infected mice. (A) The number of more than 2-fold up or down-regulated DEGs that identified from the comparison among PBS and virus-infected groups. (B) Venn diagrams of overlapping DEGs profiles for r-JY and JY-PB2-I283M-K526R group. The number indicates the mRNA count in the indicated area. (C—D) Volcano plot of DEGs in the lungs from r-JY- or JY-PB2-I283M-K526R-infected mice. The x-axis represents the $\log_2$ values of the fold change observed for each mRNA transcript, and the y-axis represents the $\log_{10}$ values of the *P*-values of the significance tests between replicates for each transcript. (D) Heatmap of the mRNA differential expression profiles in lungs from r-JY- and JY-PB2-I283M-K526R-infected mice compared with PBS-infected mice at 3 d. p.i. Co-regulated genes were clustered.

Table 2
Top 10 of up-regulated DEGs in r-JY- and JY-PB2-I283M-K526R-infected mice.

Group	Gene symbol	log2Fc	*q* value	Gene name	Gene ID
r-JY	Saa3	5.85	0.0039	serum amyloid A 3	ENSMUSG00000040026
	Anks1b	5.24	0.0039	ankyrin repeat and sterile alpha motif domain containing 1B	ENSMUSG00000058589
	Prss36	4.50	0.0039	protease, serine 36	ENSMUSG00000070371
	Ly6i	4.18	0.0039	lymphocyte antigen 6 complex, locus I	ENSMUSG00000022586
	Apod	3.59	0.0039	apolipoprotein D	ENSMUSG00000022548
	CXCL10	3.41	0.0071	chemokine (C-X-C motif) ligand 10	ENSMUSG00000034855
	Hspa1b	3.34	0.0039	heat shock protein 1B	ENSMUSG00000090877
	Ighg1	3.21	0.0071	immunoglobulin heavy constant gamma 1	ENSMUSG00000076614
	Mobp	3.14	0.0500	myelin-associated oligodendrocytic basic protein	ENSMUSG00000032517
	1700030K09Rik	3.12	0.0039	RIKEN cDNA 1700030K09 gene	ENSMUSG00000052794
JY-PB2-I283M-K526R	Irg1	8.99	0.0211	immunoresponsive gene 1	ENSMUSG00000022126
	Saa3	8.38	0.0005	serum amyloid A 3	ENSMUSG00000040026
	CXCL10	8.05	0.0005	chemokine (C-X-C motif) ligand 10	ENSMUSG00000034855
	CCL7	7.29	0.0005	chemokine (C—C motif) ligand 7	ENSMUSG00000035373
	CCL2	7.05	0.0005	chemokine (C—C motif) ligand 2	ENSMUSG00000035385
	Rsad2	6.77	0.0005	radical S-adenosyl methionine domain containing 2	ENSMUSG00000020641
	Trim30c	6.63	0.0460	tripartite motif-containing 30C	ENSMUSG00000078616
	Mx1	6.58	0.0005	MX dynamin-like GTPase 1	ENSMUSG00000000386
	Sectm1a	6.54	0.0097	secreted and transmembrane 1A	ENSMUSG00000025165
	Gm5960	6.34	0.0073	predicted gene 5960	ENSMUSG00000099775

2.8. Apoptosis assay

MDCK cells were infected with r-JY or JY-PB2-I283M-K526R at a MOI of 1. At 12, 24, and 36 h post-infection (h. p. i.), both infected and non-infected MDCKs were stained with fluorescein isothiocyanate (FITC)-conjugated annexin V and propidium iodide (PI) according to the manufacturer's instructions (BD Biosciences, San Jose, CA, USA). The stained cells were then analyzed by a caliber flow cytometry (Becton Dickinson, Franklin Lakes, NJ, USA). Early apoptotic cells are characterized by annexin V^+ and PI^- staining, later apoptotic cells by annexin V^+ and PI^+ staining, whereas necrotic cells by annexin V^- and PI^+(Qin et al., 2019). The cell proportions were analyzed using FlowJo V10 software (FlowJo LLC, Ashland, OR, USA).

2.9. Statistical analysis

Results were expressed as the means ± SD and drew with GraphPad Prism 8 software (San Diego, CA). Unpaired Student's two-sided *t*-test was employed to determine the differences between the two groups. To compare multiple groups, we performed one-way ANOVA with Tukey's post hoc test using SPSS 17.0. $^*P < 0.05$, $^{**}P < 0.01$.

3. Results

3.1. Whole-transcriptome analysis of murine lung infected with r-JY and JY-PB2-I283M-K526R virus

To gain global gene expression profiles of r-JY or JY-PB2-I283M-K526R infected mice, RNA-seq was performed to explore the transcriptomes from murine lungs at 3 d. p. i. More than 53 million 150-bp paired-end clean reads were generated. The base quality of RNA-seq reads was checked and the result showed that the base composition of each sample was equilibrious (Supplementary Fig. 1). In addition, each sample focused on exon region as shown by pie charts (Supplementary Fig. 2). Correlation of gene expression showed that each sample were able to discriminate between the two main groups of virus-infected mice (Supplementary Fig. 3). All analysis reflected that the quality of RNA-seq reads were high and sequencing data can be further analyzed.

Using the annotated genes in the murine genome database, the gene expression in lungs was quantified and compared between the control and the virus-infected groups, and differentially expressed genes (DEGs) were identified. By screening the DEGs between virus-infected groups and PBS group, we found a remarkable difference of the transcriptional host responses between two viruses at 3 d. p. i. As shown in Fig. 1A, a

Table 3
Top 10 of down-regulated DEGs in r-JY- and JY-PB2-I283M-K526R-infected mice.

Group	Gene symbol	log2Fc	*q* value	Gene name	Gene ID
r-JY	Ear-ps2	−2.50	0.0039	eosinophil-associated, ribonuclease A family, pseudogene 2	ENSMUSG00000072599
	Nppa	−2.26	0.0039	natriuretic peptide type A	ENSMUSG00000041616
	Glycam1	−2.12	0.0039	glycosylation dependent cell adhesion molecule 1	ENSMUSG00000022491
	Ang5	−2.08	0.0180	angiogenin, ribonuclease A family, member 5	ENSMUSG00000053961
	Gm13225	−2.05	0.0180	predicted gene 13225	ENSMUSG00000078503
	Cwc22	−2.00	0.0039	CWC22 spliceosome-associated protein	ENSMUSG00000027014
	Poc1a	−1.87	0.0039	POC1 centriolar protein homolog A (Chlamydomonas)	ENSMUSG00000023345
	Cd209b	−1.82	0.0202	CD209b antigen	ENSMUSG00000065987
	Il22ra2	−1.48	0.0071	interleukin 22 receptor, alpha 2	ENSMUSG00000039760
	Mb	−1.40	0.0306	myoglobin	ENSMUSG00000018893
JY-PB2-I283M-K526R	Cd209b	−4.81	0.0369	CD209b antigen	ENSMUSG00000065987
	GSTA2	−4.72	0.0337	glutathione S-transferase, alpha 2	ENSMUSG00000057933
	Gkn3	−3.81	0.0199	gastrokine 3	ENSMUSG00000030048
	Gsg1l	−3.56	0.0103	GSG1-like	ENSMUSG00000046182
	Cyp2a5	−3.46	0.0005	cytochrome P450, family 2, subfamily a, polypeptide 5	ENSMUSG00000005547
	Fmo3	−3.43	0.0005	flavin containing monooxygenase 3	ENSMUSG00000026691
	SCGB3A2	−3.38	0.0005	secretoglobin, family 3A, member 2	ENSMUSG00000038791
	Car3	−3.34	0.0005	carbonic anhydrase 3	ENSMUSG00000027559
	Sult1d1	−3.24	0.0005	sulfotransferase family 1D, member 1	ENSMUSG00000029273
	Upk2	−3.20	0.0378	uroplakin 2	ENSMUSG00000041523

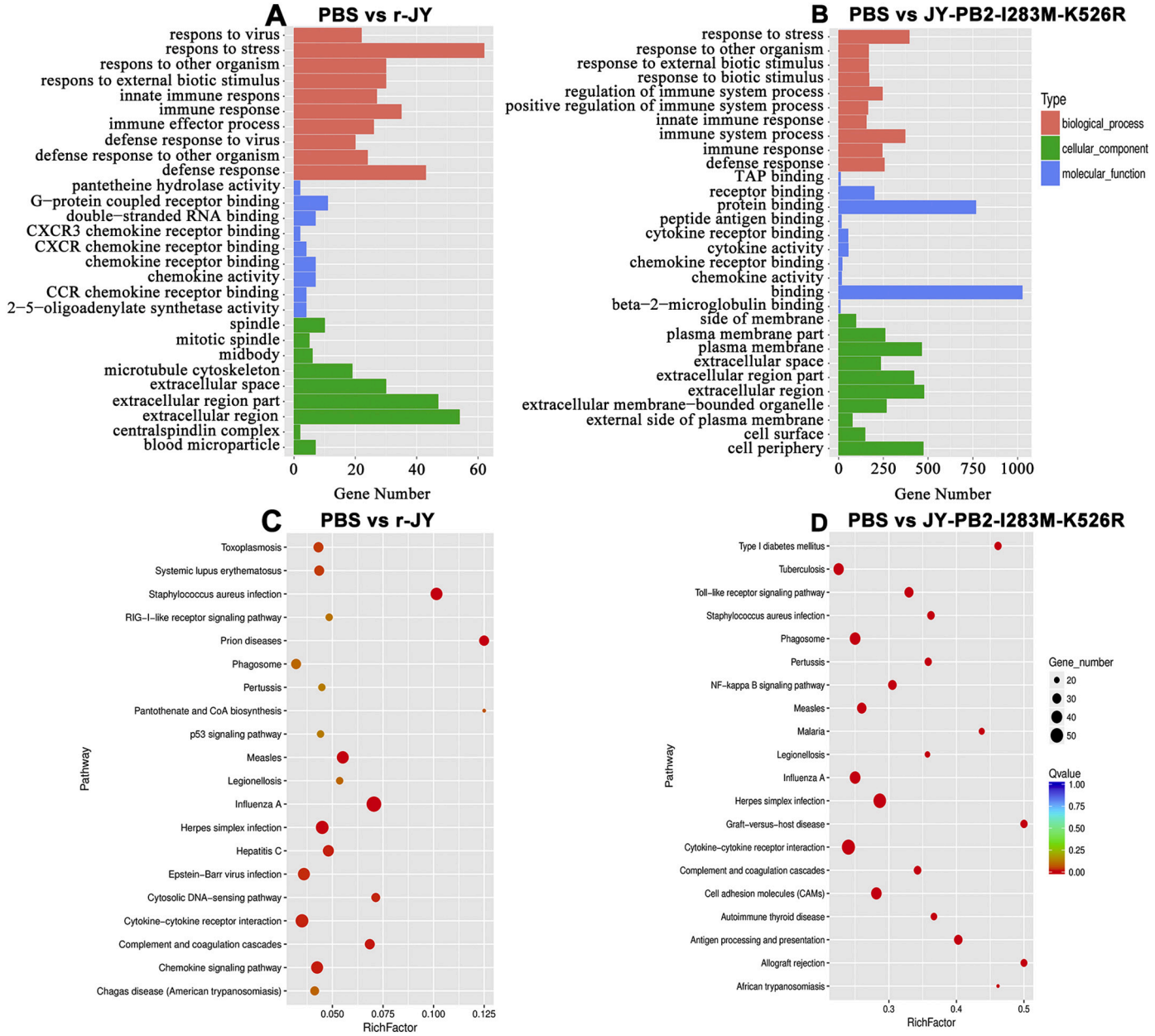

Fig. 2. The global innate immune response-related gene expression in murine lungs after r-JY and JYPB2-I283M-K526R infection. (A, B) Hierarchical clustering of expression profiles of innate immune response-related genes during infection with r-JY or JYPB2-I283M-K526R at 3 d.p.i. (A) Genes involved in the activation or trafficking of immune cells, including dendritic cells (DCs) and antigen-presenting cells (APCs), macrophages, NK cells, T lymphocytes, and cytokine responses. (B) IFN and IFN-related genes. (C) qRT-PCR analysis of representative immune-related gene expression in the lungs of mice infected with r-JY or JYPB2-I283M-K526R virus. The expression levels of each gene are normalized to that of the β-actin gene and are presented as the fold change from the expression level in PBS-treated mice. Values are means±SD for at least three independent experiments. *P < 0.05; **P < 0.01. GO and KEGG pathways analysis of the DEGs. Top 10 of GO and Top 20 of KEGG pathways analysis of the DEGs from the lungs of r-JY- (A, C) and JY-PB2-I283M-K526R-infected mice (B, D) at 3 d. p. i.

total of 1735 DEGs were stimulated by JY-PB2-I283M-K526R, whereas just 211 DEGs were from r-JY group. The number of up-regulated DEGs were higher than those of down-regulated DEGs in both groups. Of note, the up-regulated numbers of DEGs from JY-PB2-I283M-K526R-infected mice were higher than in those of r-JY-infected mice. Furthermore, a Venn diagram summarizing the distribution of DEGs showed that only 147 genes were shared by the two groups (Fig. 1B). As shown in Fig. 1C and D, the ratio of the differential expression showed a good correlation between the fold change and *p*-values (i.e. genes with a large fold change also had a low *p*-value in the group-wise comparison) in the volcano plot. And the number of DEGs of JY-PB2-I283M-K526R group was higher than those of r-JY group. Additionally, hierarchical clustering analysis indicated a good clustering of samples according to levels of similarities in the gene expression pattern. We found a clear distinction between the r-JY- and JY-PB2-I283M-K526R-infected mice, whereas the gene expression pattern from r-JY-infected mice were similar to that from PBS-infected mice (Fig. 1E).

To further analyze the characteristics of DEGs, we focused on the top 10 of significantly up- or down-regulated DEGs from r-JY- and JY-PB2-I283M-K526R-infected mice (Tables 2 and 3, or Supplementary Table S1). In comparison to the group of r-JY, the immune function-related DEGs from JY-PB2-I283M-K526R group were dramatically increased, including Irg1, Saa3, C-X-C motif chemokine 10 (CXCL-10), chemokine (C—C motif) ligand 7 (CCL7), CCL-2, and Mx1. In contrast,

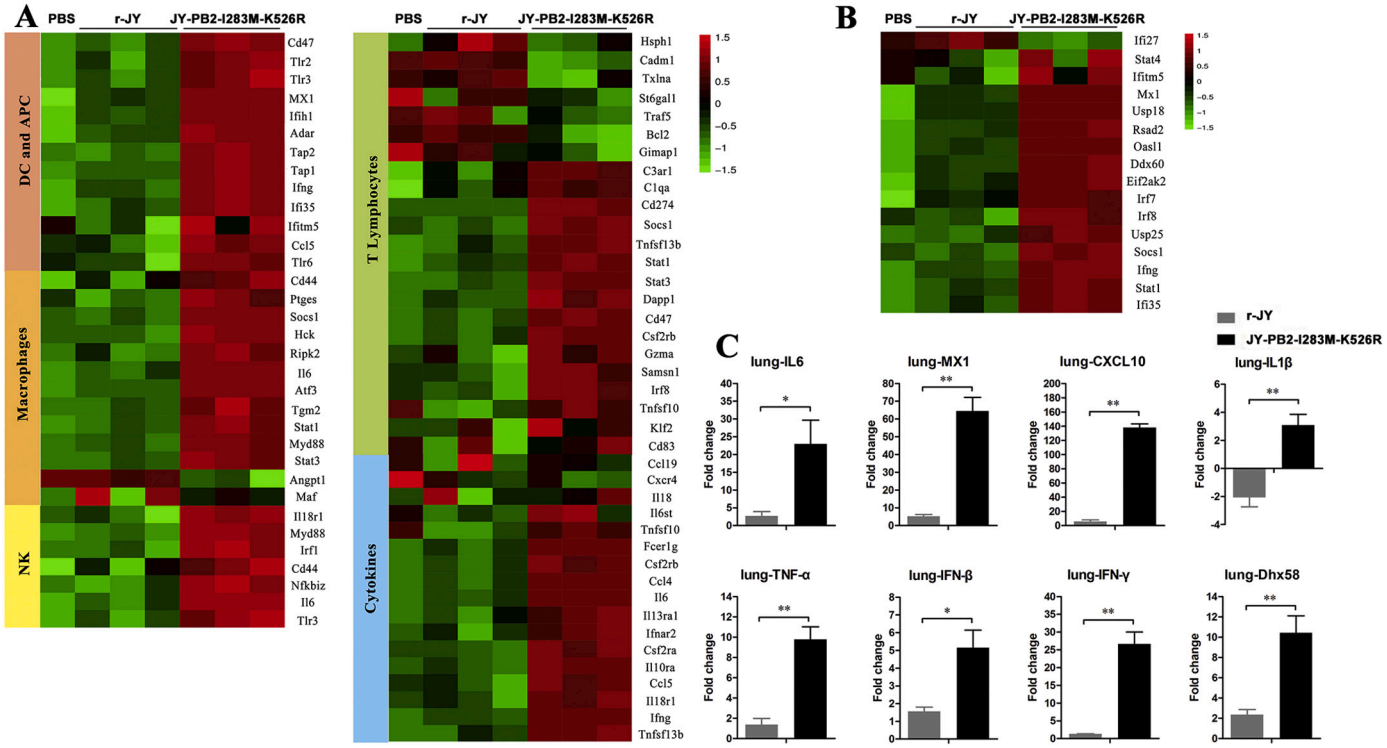

Fig. 3. The global innate immune response-related gene expression in murine lungs after r-JY and JY-PB2-I283M-K526R infection. (A, B) Hierarchical clustering of expression profiles of innate immune response-related genes during infection with r-JY or JY-PB2-I283M-K526R at 3 d. p. i. (A) Genes involved in the activation or trafficking of immune cells, including dendritic cells (DCs) and antigen-presenting cells (APCs), macrophages, NK cells, T lymphocytes, and cytokine responses. (B) IFN and IFN-related genes. (C) qRT-PCR analysis of representative immune-related gene expression in the lungs of mice infected with r-JY or JY-PB2-I283M-K526R virus. The expression levels of each gene are normalized to that of the β-actin gene and are presented as the fold change from the expression level in PBS-treated mice. Values are means±SD for at least three independent experiments. $*P < 0.05$; $**P < 0.01$.

the metabolism-related DEGs, such as Apod and Mobp, were observed in 10 most up-regulated genes of r-JY group (Table 2). Among top 10 of down-regulated DEGs, the DEGs related to organic protection (Cyp2a5, Upk2, and SCGB3A2) were observed in JY-PB2-I283M-K526R group, whereas the metabolism-related DEGs (Ear-ps2, Nppa, Ang5, Poc1a, and Mb) were observed in r-JY group (Table 3), suggesting that abnormal immune response, metabolic regulation, and organ damage may relate to the high virulence of JY-PB2-I283M-K526R virus in mice.

3.2. *PB2-I283M-K526R mutation strongly induced the expression of immune-related DEGs*

To determine the biological roles of the DEGs, a gene ontology (GO) enrichment analysis was employed. In the "biological process" term (Fig. 2 A and B), the response to stress and the defense response to virus was significantly over-expressed in both virus-infected groups. Notably, in comparison with r-JY-infected mice, more genes were found to be included in the immune system processes in the JY-PB2-I283M-K526R-infected mice. In "molecular function" term, the number of DEGs of r-JY group was small, whereas a large number of binding-related genes were observed in JY-PB2-I283M-K526R group, suggesting a complicated mechanism of protein binding was involved in the interaction between mutant virus and host. To investigate possible biological interactions of DEGs and identify important functional networks, datasets representing genes with altered expression profiles were analyzed by using KEGG pathway method (Fig. 2C and D). Influenza A virus pathway was observed in both groups, suggesting a successful establishment of virus infection. However, in comparison with r-JY-infected mice, DEGs from JY-PB2-I283M-K526R-infected mice were mainly enriched in immune-related pathways, such as "Toll-like receptor signaling pathway", "NF-kappa B signaling pathway", "Cell adhesion molecules", and "Antigen processing and presentation". Taken together, the GO and KEGG analysis implied that the PB2-I283M-K526R mutation of H5N8 virus strongly induced the immune-related DEGs expression.

3.3. *PB2-I283M-K526R mutation augments the innate immune response in murine lungs*

We next focused on analyzing the expression patterns of genes involved in the "innate immune response". As shown in Fig. 3A, "innate immune response" genes were divided in 5 categories. Heat map profiles revealed a number of genes associated with this function expressed at higher levels in mice infected with JY-PB2-I283M-K526R than in that infected with r-JY. Moreover, higher expression levels of these genes, relative to expression in PBS-infected controls, during JY-PB2-I283M-K526R infection than during r-JY infection. In addition, interferon (IFN) is involved in innate immune response, therefore, IFN and IFN-related genes were also analyzed. They expressed at higher levels in JY-PB2-I283M-K526R group than in r-JY group (Fig. 3B). Based on the results of RNA-seq analysis, we further determined the impact of mutation in PB2-I283M-K526R on the innate immune response by profiling the expression of a set of representative genes in the lungs of virus-infected mice. Overall, JY-PB2-I283M-K526R elicited a stronger cytokine response than r-JY, and the expression of MX1, CXCL10, and IFN-γ was more highly activated with >10-folds by JY-PB2-I283M-K526R than by r-JY (Fig. 3C). Collectively, these results indicated that the PB2-I283M-K526R mutation elicited a strong innate immune response in murine lungs, which may contribute to the increased virulence in mice.

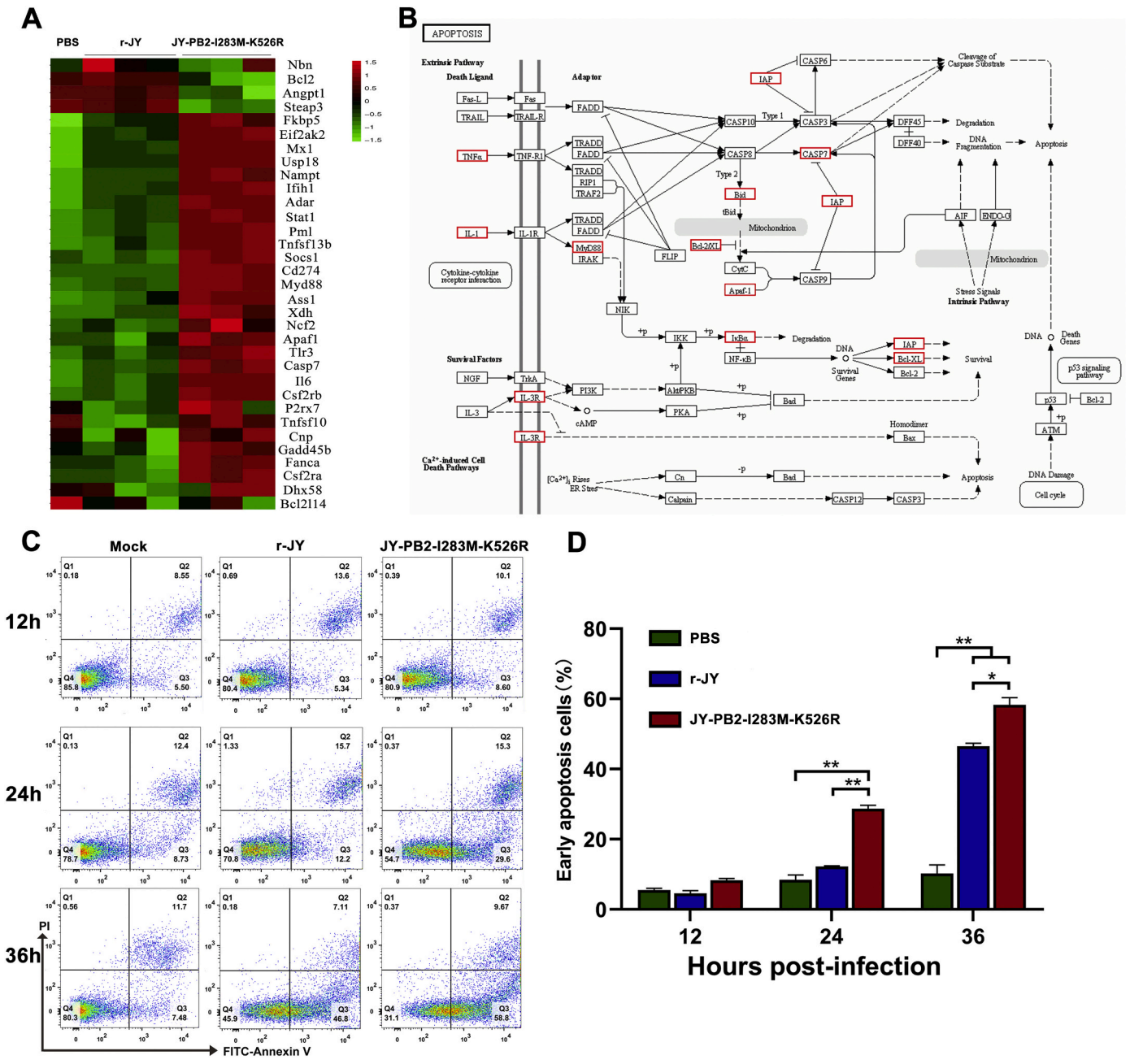

Fig. 4. PB2-I283M-K526R mutation accelerates the level of cell apoptosis. (A) Heatmap shows the hierarchical clustering of transcriptional profiles of apoptosis-related genes during infection with r-JY or JY-PB2-I283M-K526R at 3 d. p. i. (B) The genes and their functional relationships within the apoptotic signaling pathway in the lungs of mice infected with JY-PB2-I283M-K526R at 3 d. p. i. Genes highlighted in red were up-regulated. (C, D) Flow cytometry analysis of early apoptosis of MDCK infected with r-JY or JY-PB2-I283M-K526R (MOI = 1) at 12, 24, and 36 h. p. i. Apoptosis cells are those with annexin V^+ and low PI^- staining (early stage). (D) Quantitative analysis of early apoptosis cells from (C). Values is presented as the mean ± SD of three independent experiments. $^*P < 0.05$, $^{**}P < 0.01$.

3.4. PB2-I283M-K526R mutation accelerates the level of cell apoptosis

Influenza virus infection induces cell apoptosis, resulting in cellular and organ damages, subsequently leading to lethal pathogenicity (Hu et al., 2015). Heat map profiles revealed higher expression levels of apoptosis-related genes in the group of JY-PB2-I283M-K526R than that in r-JY at 3 d. p. i. (Fig. 4A). Bcl2, a negative regulator of apoptosis (Mehrbod et al., 2019), was decreased in JY-PB2-I283M-K526R group compared with control or r-JY group. Notably, high activation of multiple genes involved in the tumor necrosis factor (TNF)-mediated apoptosis pathway during JY-PB2-I283M-K526R infection (Fig. 4B). To determine the effect of mutant virus on virus-induced apoptosis at early stage and validate the microarray results, MDCK cells were inoculated with r-JY, JY-PB2-I283M-K526R, or mock, and cell apoptosis was measured by using double staining with annexin V and PI. As shown in Fig. 4C and D, the two viruses significantly induced more early apoptotic cells than mock at 24 and 36 h. p. i. Moreover, the proportion of early apoptotic cells was significantly higher in JY-PB2-I283M-K526R-infected cells than r-JY at both time points.

4. Discussion

Our previous study showed that synergistic effect of amino acid residues 283M and 526R in the PB2 protein was responsible for

enhancing virulence of HPAI H5N8 viruses in mice (Wang et al., 2017). However, the underlying pathogenesis is not clear. Therefore, in this study, we continue to use r-JY virus and its mutant (JY-PB2-I283M-K526R) with a combined I283M-K526R in PB2 protein to analyze the effect of above mutation to global host response by using RNA-seq technology. We found that PB2-I283M-K526R mutation strongly induced more DEG expressions, which mainly related with innate immune response by GO and KEGG analysis. We also found that PB2-I283M-K526R mutation accelerated the levels of cell apoptosis by a heat map analysis of apoptosis-related DEGs and an apoptosis assay *in vitro*. These remarkable changes of innate immune response and apoptosis might be key factors for an increased pathogenicity in mammals.

The innate immune system constitutes the first line of host defense during infection, which relies on recognition of conserved structures on pathogens, termed pathogen-associated molecular patterns (PAMPs), through various pattern recognition receptors (PRRs), such as toll-like receptors (TLRs) and RIG-I-like receptors (RLRs) (Akira et al., 2006; Medzhitov and Janeway Jr., 2000). However, the over-intense virus-induced innate immune response is not beneficial to host. H5 AIV-induced cytokine dysregulation may be a contributory factor to the mammalian pathogenesis (Mok et al., 2009). Based on our RNA-seq analysis, we observed that a modest secretion of inflammatory molecules in the organs of JY-infected mice, whereas a robust secretion of inflammatory molecules in those of JY-PB2-I283M-K526R-infected mice. Moreover, the cytokines/chemokines levels, especially MX1, CXCL10, and IFN-γ, performed by qRT-PCR were all up-regulated upon mutant virus infection, which was in line with the global innate immune response-related mRNA levels. Our previous study showed that JY-PB2-I283M-K526R-infected group displayed a more virus-load in murine lungs than JY-infected group (Wang et al., 2017), which will further stimulate a broader inflammatory response. The strong innate immune response can trigger inflammation to become excessive, driven by the overproduction of inflammatory mediators, named “cytokine storm”, which can rapidly kill cells, causing severe tissue damage while precipitating organ dysfunction and failure (Murphy, 2017). The interferon (IFN) system plays a key role in inducing an antiviral state and contributes to the subsequent antigen specific adaptive immune response (Killip et al., 2015). Notably, IFNs also important pro-inflammatory cytokines in the form of severe cytokine storm during influenza infection (Liu et al., 2016). Particularly, type I and III IFNs in the primary cytokine wave and Type II IFNs (IFN-γ) in the secondary cytokine wave were remarkably induced (Guo and Thomas, 2017). Our data demonstrated that DEGs from JY-PB2-I283M-K526R-infected mice facilitated a severe increase in IFN-γ production, implying that a strong cytokine storm was induced in the second stage. Additionally, PB2-I283M-K526R mutation sharply upregulated the expression of IFN-γ-inducible protein 10 (IP10/CXCL10), which can lead to a large recruitment of immune cells and robust immune activation.

Influenza virus can induce apoptosis in multiple cell types (Brydon et al., 2003; Hinshaw et al., 1994; Hu et al., 2015; Morris et al., 1999; Nichols et al., 2001; Price et al., 1997). Excessive apoptosis then causes organ damage, contributing to virus pathogenicity (Brydon et al., 2005; McLean et al., 2008). Previously, PA gene of influenza virus (A/California/04/2009) is also associated with virus-induced apoptosis (Desmet et al., 2013). PB1-F2, located at the PB1 protein, is a pro-apoptotic protein that induces cell apoptosis via the mitochondrial pathway (Zamarin et al., 2005). PB1 and PB2 also are involved in the induction of apoptosis. Different cell apoptosis levels induced by H5N1 virus related with amino acid changes in PB1 and PB2 (Morris et al., 2005). Our data suggested that PB2-I283M-K526R mutation accelerated the levels of cell apoptosis, which may be associated with the increased virulence in mice. Notably, TNF-α and TNF-mediated apoptosis pathway during JY-PB2-I283M-K526R infection was involved in our study. TNF is also called a death ligand, which can trigger various caspases activation. Caspases also cleaves BH3 interacting domain death agonist protein (Bid), which mediates mitochondrial damage and then results in the loss of mitochondrial membrane potential to release cytochrome-c to the cytosol. The released cytochrome-c can bind to apoptotic protease activating factor 1 (Apaf1), an adaptor protein, to form “Apoptosome”(Fujikura and Miyazaki, 2018; Mehrbod et al., 2019). Consistently, Caspase 7, Bid, and Apaf1 were remarkably upregulated in the group of JY-PB2-I283M-K526R. However, further studies are needed to elucidate the underlying mechanism of PB2-I283M-K526R mutation-associated apoptosis activity.

In summary, the present study demonstrates that PB2-I283M-K526R of H5N8 subtype of HPAIV exacerbated innate immune response and the levels of cell apoptosis, which may together contribute to the higher pathogenicity of PB2-I283M-K526R mutants in mammals. Thus, our study defines the role of the novel PB2-I283M-K526R mutation in the pathogenesis of H5N8 subtype AIV and has important implications for understanding the variable pathogenesis of AIV. Additional studies are required to understand whether these results can be generalized to other influenza virus subtypes or whether they are unique to H5 subtypes.

Author statement

Sujuan Chen, Xiao Wang, Daxin Peng and Xiufan Liu for conceptualization; Xiao Wang, Xinyu Miao and Xiang Su for investigation; Sujuan Chen, Tao Qin, XiaoWang and Daxin Peng for formal analysis; XiaoWang and Tao Qin for writing - original draft.

Declaration of Competing Interest

The authors have declared that no competing interest exists.

Acknowledgements

This work was supported by the National Key R&D Project (2016YFD0500202), the National Natural Science Foundation of China (31872477, 31872473, 31602057, 31802212), the Jiangsu Provincial Natural Science Fund for Excellent Young Scholars (BK20200105) for Tao Qin, the Jiangsu Agriculture Science and Technology Innovation Fund (CX(18)3018), the Key R&D Project of Jiangsu Province (BE2018358), Six Talent Peaks Project in Jiangsu Province (NY-131), the High Level Talent Support Plan of Yangzhou University, and a project funded by the Priority Academic Program Development of Jiangsu Higher Education (PAPD).

Appendix A. Supplementary data

Supplementary data to this article can be found online at https://doi.org/10.1016/j.meegid.2020.104672.

References

Akira, S., Uematsu, S., Takeuchi, O., 2006. Pathogen recognition and innate immunity. Cell 124, 783–801.

Baskin, C.R., Bielefeldt-Ohmann, H., Tumpey, T.M., Sabourin, P.J., Long, J.P., Garcia-Sastre, A., Tolnay, A.E., Albrecht, R., Pyles, J.A., Olson, P.H., Aicher, L.D., Rosenzweig, E.R., Murali-Krishna, K., Clark, E.A., Kotur, M.S., Fornek, J.L., Proll, S., Palermo, R.E., Sabourin, C.L., Katze, M.G., 2009. Early and sustained innate immune response defines pathology and death in nonhuman primates infected by highly pathogenic influenza virus. Proc. Natl. Acad. Sci. U. S. A. 106, 3455–3460.

Brydon, E.W., Smith, H., Sweet, C., 2003. Influenza A virus-induced apoptosis in bronchiolar epithelial (NCI-H292) cells limits pro-inflammatory cytokine release. J. Gen. Virol. 84, 2389–2400.

Brydon, E.W., Morris, S.J., Sweet, C., 2005. Role of apoptosis and cytokines in influenza virus morbidity. FEMS Microbiol. Rev. 29, 837–850.

Cameron, C.M., Cameron, M.J., Bermejo-Martin, J.F., Ran, L., Xu, L., Turner, P.V., Ran, R., Danesh, A., Fang, Y., Chan, P.K., Mytle, N., Sullivan, T.J., Collins, T.L., Johnson, M.G., Medina, J.C., Rowe, T., Kelvin, D.J., 2008. Gene expression analysis of host innate immune responses during Lethal H5N1 infection in ferrets. J. Virol. 82, 11308–11317.

Cloonan, N., Forrest, A.R., Kolle, G., Gardiner, B.B., Faulkner, G.J., Brown, M.K., Taylor, D.F., Steptoe, A.L., Wani, S., Bethel, G., Robertson, A.J., Perkins, A.C., Bruce, S.J., Lee, C.C., Ranade, S.S., Peckham, H.E., Manning, J.M., McKernan, K.J.,

Grimmond, S.M., 2008. Stem cell transcriptome profiling via massive-scale mRNA sequencing. Nat. Methods 5, 613–619.
de Jong, M.D., Simmons, C.P., Thanh, T.T., Hien, V.M., Smith, G.J., Chau, T.N., Hoang, D.M., Chau, N.V., Khanh, T.H., Dong, V.C., Qui, P.T., Cam, B.V., Ha Do, Q., Guan, Y., Peiris, J.S., Chinh, N.T., Hien, T.T., Farrar, J., 2006. Fatal outcome of human influenza A (H5N1) is associated with high viral load and hypercytokinemia. Nat. Med. 12, 1203–1207.
Desmet, E.A., Bussey, K.A., Stone, R., Takimoto, T., 2013. Identification of the N-terminal domain of the influenza virus PA responsible for the suppression of host protein synthesis. J. Virol. 87, 3108–3118.
Fujikura, D., Miyazaki, T., 2018. Programmed cell death in the pathogenesis of influenza. Int. J. Mol. Sci. 19.
Global Consortium for, H.N., Related Influenza, V, 2016. Role for migratory wild birds in the global spread of avian influenza H5N8. Science 354, 213–217.
Guo, X.Z.J., Thomas, P.G., 2017. New fronts emerge in the influenza cytokine storm. Semin. Immunopathol. 39, 541–550.
Hinshaw, V.S., Olsen, C.W., Dybdahl-Sissoko, N., Evans, D., 1994. Apoptosis: a mechanism of cell killing by influenza A and B viruses. J. Virol. 68, 3667–3673.
Hu, J., Mo, Y., Wang, X., Gu, M., Hu, Z., Zhong, L., Wu, Q., Hao, X., Hu, S., Liu, W., Liu, H., Liu, X., Liu, X., 2015. PA-X decreases the pathogenicity of highly pathogenic H5N1 influenza A virus in avian species by inhibiting virus replication and host response. J. Virol. 89, 4126–4142.
Juranic Lisnic, V., Babic Cac, M., Lisnic, B., Trsan, T., Mefferd, A., Das Mukhopadhyay, C., Cook, C.H., Jonjic, S., Trgovcich, J., 2013. Dual analysis of the murine cytomegalovirus and host cell transcriptomes reveal new aspects of the virus-host cell interface. PLoS Pathog. 9, e1003611.
Killip, M.J., Fodor, E., Randall, R.E., 2015. Influenza virus activation of the interferon system. Virus Res. 209, 11–22.
Li, X., Brock, G.N., Rouchka, E.C., Cooper, N.G.F., Wu, D., O'Toole, T.E., Gill, R.S., Eteleeb, A.M., O'Brien, L., Rai, S.N., 2017. A comparison of per sample global scaling and per gene normalization methods for differential expression analysis of RNA-seq data. PLoS One 12, e0176185.
Liu, Q., Zhou, Y.H., Yang, Z.Q., 2016. The cytokine storm of severe influenza and development of immunomodulatory therapy. Cell. Mol. Immunol. 13, 3–10.
Ma, J., Wei, L., Li, J., Li, H., 2018. The analysis of genes and phytohormone metabolic pathways associated with leaf shape development in *Liriodendron chinense* via de novo transcriptome sequencing. Genes (Basel) 9.
McLean, J.E., Ruck, A., Shirazian, A., Pooyaei-Mehr, F., Zakeri, Z.F., 2008. Viral manipulation of cell death. Curr. Pharm. Des. 14, 198–220.
Medzhitov, R., Janeway Jr., C., 2000. Innate immunity. N. Engl. J. Med. 343, 338–344.
Mehrbod, P., Ande, S.R., Alizadeh, J., Rahimizadeh, S., Shariati, A., Malek, H., Hashemi, M., Glover, K.K.M., Sher, A.A., Coombs, K.M., Ghavami, S., 2019. The roles of apoptosis, autophagy and unfolded protein response in arbovirus, influenza virus, and HIV infections. Virulence 10, 376–413.
Mei, B., Ding, X., Xu, H.Z., Wang, M.T., 2014. Global gene expression changes in human peripheral blood after H7N9 infection. Gene 551, 255–260.
Mok, K.P., Wong, C.H.K., Cheung, C.Y., Chan, M.C., Lee, S.M.Y., Nicholls, J.M., Guan, Y., Peiris, J.S.M., 2009. Viral genetic determinants of H5N1 influenza viruses that contribute to cytokine dysregulation. J. Infect. Dis. 200, 1104–1112.
Morris, S.J., Price, G.E., Barnett, J.M., Hiscox, S.A., Smith, H., Sweet, C., 1999. Role of neuraminidase in influenza virus-induced apoptosis. J. Gen. Virol. 80 (Pt 1), 137–146.
Morris, S.J., Nightingale, K., Smith, H., Sweet, C., 2005. Influenza A virus-induced apoptosis is a multifactorial process: exploiting reverse genetics to elucidate the role of influenza A virus proteins in virus-induced apoptosis. Virology 335, 198–211.
Mortazavi, A., Williams, B.A., McCue, K., Schaeffer, L., Wold, B., 2008. Mapping and quantifying mammalian transcriptomes by RNA-Seq. Nat. Methods 5, 621–628.
Murphy, E., 2017. An effective treatment strategy for cytokine storm in severe influenza. Am. Lab. 49, 23.
Nichols, J.E., Niles, J.A., Roberts Jr., N.J., 2001. Human lymphocyte apoptosis after exposure to influenza A virus. J. Virol. 75, 5921–5929.
Park, S.J., Kumar, M., Kwon, H.I., Seong, R.K., Han, K., Song, J.M., Kim, C.J., Choi, Y.K., Shin, O.S., 2015. Dynamic changes in host gene expression associated with H5N8 avian influenza virus infection in mice. Sci. Rep. 5, 16512.
Peiris, J.S., Yu, W.C., Leung, C.W., Cheung, C.Y., Ng, W.F., Nicholls, J.M., Ng, T.K., Chan, K.H., Lai, S.T., Lim, W.L., Yuen, K.Y., Guan, Y., 2004. Re-emergence of fatal human influenza A subtype H5N1 disease. Lancet 363, 617–619.
Perrone, L.A., Plowden, J.K., Garcia-Sastre, A., Katz, J.M., Tumpey, T.M., 2008. H5N1 and 1918 pandemic influenza virus infection results in early and excessive infiltration of macrophages and neutrophils in the lungs of mice. PLoS Pathog. 4, e1000115.
Price, G.E., Smith, H., Sweet, C., 1997. Differential induction of cytotoxicity and apoptosis by influenza virus strains of differing virulence. J. Gen. Virol. 78 (Pt 11), 2821–2829.
Qin, T., Ma, R., Yin, Y., Miao, X., Chen, S., Fan, K., Xi, J., Liu, Q., Gu, Y., Yin, Y., Hu, J., Liu, X., Peng, D., Gao, L., 2019. Catalytic inactivation of influenza virus by iron oxide nanozyme. Theranostics 9, 6920–6935.
Schmittgen, T.D., Zakrajsek, B.A., Mills, A.G., Gorn, V., Singer, M.J., Reed, M.W., 2000. Quantitative reverse transcription-polymerase chain reaction to study mRNA decay: comparison of endpoint and real-time methods. Anal. Biochem. 285, 194–204.
Szretter, K.J., Gangappa, S., Lu, X., Smith, C., Shieh, W.J., Zaki, S.R., Sambhara, S., Tumpey, T.M., Katz, J.M., 2007. Role of host cytokine responses in the pathogenesis of avian H5N1 influenza viruses in mice. J. Virol. 81, 2736–2744.
Trapnell, C., Roberts, A., Goff, L., Pertea, G., Kim, D., Kelley, D.R., Pimentel, H., Salzberg, S.L., Rinn, J.L., Pachter, L., 2012. Differential gene and transcript expression analysis of RNA-seq experiments with TopHat and cufflinks. Nat. Protoc. 7, 562–578.
Wang, Y., Lupiani, B., Reddy, S.M., Lamont, S.J., Zhou, H., 2014. RNA-seq analysis revealed novel genes and signaling pathway associated with disease resistance to avian influenza virus infection in chickens. Poult. Sci. 93, 485–493.
Wang, X., Meng, F., Wang, D., Liu, X., Chen, S., Qin, T., Peng, D., Liu, X., 2016. Characteristics of two highly pathogenic avian influenza H5N8 viruses with different pathogenicity in mice. Arch. Virol. 161, 3365–3374.
Wang, X., Chen, S., Wang, D., Zha, X., Zheng, S., Qin, T., Ma, W., Peng, D., Liu, X., 2017. Synergistic effect of PB2 283M and 526R contributes to enhanced virulence of H5N8 influenza viruses in mice. Vet. Res. 48, 67.
WHO/GIP, 2020. Cumulative Number of Confirmed Human Cases for Avian Influenza A (H5N1) Reported to WHO.
Zamarin, D., Garcia-Sastre, A., Xiao, X.Y., Wang, R., Palese, P., 2005. Influenza virus PB1-F2 protein induces cell death through mitochondrial ANT3 and VDAC1. PLoS Pathog. 1, 40–54.
Zhang, N., Bao, Y.J., Tong, A.H., Zuyderduyn, S., Bader, G.D., Malik Peiris, J.S., Lok, S., Lee, S.M., 2018. Whole transcriptome analysis reveals differential gene expression profile reflecting macrophage polarization in response to influenza A H5N1 virus infection. BMC Med. Genet. 11, 20.
Zou, W., Chen, D., Xiong, M., Zhu, J., Lin, X., Wang, L., Zhang, J., Chen, L., Zhang, H., Chen, H., Chen, M., Jin, M., 2013. Insights into the increasing virulence of the swine-origin pandemic H1N1/2009 influenza virus. Sci. Rep. 3, 1601.